# Cellular sticking can strongly reduce complex binding by speeding dissociation

Caitlin M. Davis<sup>1,2,†,\*</sup> and Martin Gruebele<sup>1,2,3,\*</sup>

<sup>1</sup>Department of Chemistry, <sup>2</sup>Department of Physics, and <sup>3</sup>Center for Biophysics and Quantitative Biology, University of Illinois at Urbana-Champaign, Urbana, IL 61801 USA

KEYWORDS. Fluorescence Resonance Energy Transfer (FRET), Laser-Induced Temperature-Jump, Macromolecular Crowding, Quinary Interactions, RNA-Protein Binding, U1 Small Nuclear Ribonucleoprotein (U1 snRNP), U1 Small Nuclear Ribonucleoprotein A (U1A).

ABSTRACT: While extensive studies have been carried out to determine protein-RNA binding affinities, mechanisms and dynamics in vitro, such studies do not take into consideration the effect of the many weak non-specific interactions in a cell filled with potential binding partners. Here we experimentally tested the role of the cellular environment on affinity and binding dynamics between a protein and RNA in living U-2 OS cells. Our model system is the spliceosomal protein U1A and its binding partner SL2 of the U1 snRNA. The binding equilibrium was perturbed by a laser-induced temperature jump and monitored by Förster resonance energy transfer. The apparent binding affinity in live cells was reduced by up to two orders of magnitude compared to in vitro. The measured in-cell dissociation rate coefficients were up to two orders of magnitude larger, whereas no change in the measured association rate coefficient was observed. The latter is not what would be anticipated due to macromolecular crowding or non-specific sticking of the un-complexed U1A and SL2 in the cell. A quantitative model fits our experimental results with the major cellular effect being that sticking reduces cellular concentrations of free U1A, free SL2, and their complex. U1A and SL2 sticking to cellular components are capable of binding, just not as strongly as the free complex. This observation suggests that high binding affinities measured or designed in vitro are necessary for proper binding in vivo where competition with many non-specific interactions exists, especially for strongly interacting species with high charge or large hydrophobic surface areas.

# INTRODUCTION

Protein interactions are critical for most cellular functions, including signal transduction, cellular regulation, and enzyme catalysis. These interactions lie on a continuum from strong sub-nanomolar to weak millimolar equilibrium dissociation constants ( $K_d$ ), that can be measured accurately in vitro and in cellulo.<sup>1–4</sup> Yet this static view of the complex, ignores the kinetic nature of binding, the association rate ( $k_{on}$ ) and dissociation rate ( $k_{off}$ ).<sup>5</sup> How changes in binding and unbinding kinetics differentially contribute to  $K_d$  is key to understanding how the cell modulates complex lifetimes to control signal transduction, regulatory processes, and pharmaceutical efficacy.<sup>6,7</sup>

Because it is technically challenging to initiate reactions in cells, fast kinetic binding measurements of proteins in living cells are scarce. Using fluorescence to determine concentrations, Förster resonance energy transfer (FRET) as a ratiometric probe of complex formation, and microinjection to initiate the binding interaction, the TEM1-BLIP complex was found to have at most two-fold reduced association rates in cells and in dilute solutions.<sup>3</sup> Time-lapse imaging following fluorescently labeled ParM found similar polymerization and de-polymerization rates in cells and in vitro.<sup>8</sup> Another approach used bioluminescence resonance energy transfer (BRET) to measure ligand-binding kinetics at the A<sub>3</sub>AR in living cells but was not compared to dilute conditions.<sup>9</sup>

Here we demonstrate a new temperature-jump based approach to quantify binding affinity and kinetics inside living

U-2 OS bone cancer cells. First, we designed a FRET labeling strategy for our model system in vitro. We selected the spliceosomal protein U1A and its binding partner stem loop 2 (SL2) of U1 small nuclear RNA (snRNA) as our model system because it is one of the most widely studied RNA recognition motifs (Figure 1). 10-12 Fluorescence was used to quantify cellular concentrations of protein and RNA. 1,3 Fast relaxation imaging (FReI), fluorescence microscopy coupled to a laserinduced temperature jump, perturbed the binding interaction and measured the association-dissociation equilibrium with ~100 ms time resolution. From these measurements we are able to quantify the binding affinity, association, and dissociation rate coefficients for the U1A-SL2 complex in U-2 OS cells. In- cell measurements are compared to complementary in vitro experiments in dilute buffer and cellular mimics of electrostatics, crowding, and sticking.

For the case of U1A-SL2 RNA we find significant differences between measurements of affinity and kinetics in-cell and in vitro; the apparent dissociation constant and dissociation rate are increased by up to two orders of magnitude while the association rate is nearly unchanged. These differences cannot be explained by crowding or electrostatics alone. Instead, sticking of the complex to the cellular matrix speeds up its dissociation, while the longer-lived 'unstuck' complex becomes more scarce. The large surface charges on the RNA binding protein and RNA likely make them particularly sus-

ceptible to sticking, unlike the cases studied previously with smaller changes in equilibrium. Our results show that binding can be influenced in unexpected ways inside cells when the species involved are strongly interacting, such as highly charged nucleic acids, globular proteins or disordered proteins.

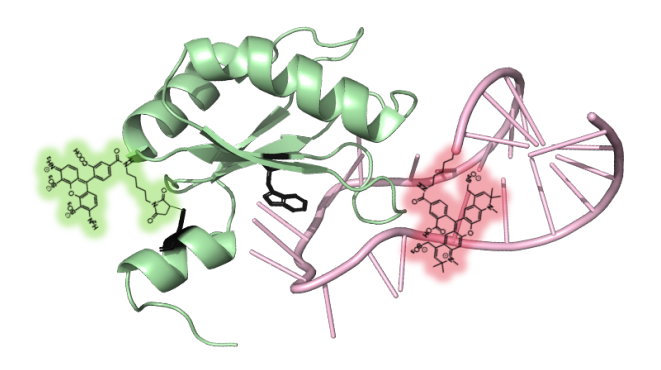


**Figure 1.** Schematic representation of the U1A-SL2 complex with FRET labels. U1A (green) is fluorescently labeled at the I94C residue using Alexa Fluor 488 C5 maleimide. Alexa Fluor 594 succinimidyl ester is attached to SL2 (red) through a 5' amino modifier C6 group. The ribbon structure of the 25 nucleotide SL2 hairpin bound to the N-terminal domain of U1A (aa 1-102) [PDB ID: 4PKD] and U1A point mutations F56W I94C (black sticks) were generated in VMD.<sup>13</sup>

#### EXPERIMENTAL SECTION

**Protein Engineering and Expression**. The expression vector for the N-terminal domain of U1A was a gift from Kiyoshi Nagai. <sup>14</sup> For purification, it contains a Ni affinity His-tag with a thrombin cleavage site at the N-terminus. Site-directed mutagenesis was performed to obtain a U1A double mutant (F56W/I94C) and mutations were confirmed by sequencing. The F56W mutation was incorporated for comparison with previous in vitro studies. <sup>15–17</sup> The I94C mutation was incorporated near the C-terminus for fluorescent dye conjugation (Figure 1).

U1A was expressed and purified as previously reported.<sup>17</sup> The histidine tag was removed by thrombin cleavage. 5 mM 2-mercaptoethanol was added to all purification and storage buffers (10 mM potassium phosphate, 50 mM KCl pH 7) to limit protein dimerization. Protein purity was assessed by SDS-PAGE and molecular weight confirmed by low-resolution electrospray ionization mass spectrometry.

**Dye Conjugation**. The reaction buffer (10 mM potassium phosphate, 50 mM KCl pH 7) was degassed for at least one hour. 50 nanomoles of U1A in degassed buffer was prepared at a final concentration of 50 uM with 10-fold excess of Tris(2-carboxyethyl)phosphine (TCEP). The reduction proceeded under nitrogen and constant stirring for 2 hours at room temperature. Alexa-488-C5-maleimide (Invitrogen) or Alexa-594-C5-maleimide (Invitrogen) was prepared at 10 mM concentration in DMSO. A 10-fold excess of dye was added to the reaction and it proceeded overnight at room temperature. Excess dye was removed by a 3,000 MWCO centrifugal filter (Millipore). The molecular weight of the dye-labeled protein was confirmed by low-resolution electrospray ionization mass spectrometry and labeling efficiency was assessed by UV spectroscopy (>95% yield).

Dye labeled SL2 RNA constructs were purchased from Integrated DNA Technologies (IDT). The SL2 construct, GGG UAU CCA UUG CAC UCC GGA UGC C, was labeled with Alexa 488 or Alexa 594 at the 5' (Figure 1) or 3' end via an NHS ester modification.

Cell Culture and Microinjection. Human bone osteosar-coma epithelial cells (U-2 OS) were cultured and grown on coverslips in DMEM (Corning) + 1% penicillin-streptomycin (Corning) + 10% fetal bovine serum (FBS, ThermoFisher Scientific) media. At 50% confluency the culture media was replaced with Opti-MEM reduced serum media (Gibco) supplemented with 10% FBS. Cells were microinjected with U1A, SL2, or 1:1 U1A-SL2 complex using an Eppendorf FemtoJet microinjector. Excess dye was washed, and an imaging chamber was prepared by sandwiching the cells between a coverslip (Fisherbrand, No. 1.5) and microscope slide (Fisherbrand, 1 mm) with a 120 μm spacer (Grace Bio-Labs, Bend, OR). Identical imaging chambers were used for in vitro and in cell studies.

Fast Relaxation Imaging (FReI). The FReI apparatus has been described previously. Briefly, an infrared laser was used to rapidly perturb the binding equilibrium via heating on a timescale faster than the dynamics of interest. Fluorescence microscopy was then used to probe the relaxation kinetics of binding. A computer controlled, continuous-wave 2  $\mu$ m laser (AdValue Photonics, Tucson, AZ) produced a step-function shaped temperature perturbation. The magnitude of the temperature jump was calculated using the temperature-dependent quantum yield of mCherry excited between 565 and 598 nm. Phe stepped temperature perturbation began at  $\approx 21$  °C and increased to  $\approx 45$  °C in 3 °C steps. The complex was given  $\approx 9$  s ( $\approx 10$  relaxation lifetimes) to relax to its new equilibrium following each jump.

The change in signal induced by the temperature jump was imaged over the whole cell in real time by fluorescence microscopy. A white LED (Prizmatix, UHP-T2-LED-White) excited the donor label for FRET excitation by passing the light through an ET470/40x bandpass filter (Chroma, Bellows Falls, VT) and T495lpxt dichroic (chroma). Alternatively, to excite the acceptor label an ET580/25x bandpass filter (Chroma) and T600lpxr dichroic (Chroma) were used. The excitation was focused onto the sample with a microscopy objective (Zeiss, 63x/0.85 NA N-Achroplan) and the emission was passed through an ET500lp filter (Chroma) and split into two channels (donor/green and acceptor/red) by a T600lpxr dichroic (Chroma) onto a CMOS camera (Lumenera, LT225 NIR/SCI CMOS detector). Images were collected at a frame rate of 60 Hz with 16 ms integration times. Instrument control and data collection were controlled using a LabView (National Instruments, Austin, TX) computer program. Data collected with the CMOS detector was converted to a MATLAB (MathWorks, Natick, MA) compatible format. MATLAB was used to separate and align the channels and segment cell images into nucleus, cytoplasm, and background using Otsu's method.20

Analysis of Thermodynamic Data. Temperature induced dissociation equilibrium of the complex was measured using a FP-8300 Spectrofluorometer (Jasco, Easton, MD) or the average of the final 4 seconds after the jump when equilibrium has essentially been reached. Thermodynamic data was plotted as the FRET efficiency of the donor (D) and acceptor (A) intensities (A/[A+D]) vs. temperature. The resulting temperature

titration was fit to the fractional saturation of a bimolecular

$$S_N(T) = \frac{([P]_T + [R]_T + K_d) - (([P]_T + [R]_T + K_d)^2 - 4[P]_T [R]_T)^{1/2}}{2[P]_T}$$
(1a)

$$S(T) = S_F - (S_F - S_R)S_N(T)$$
 (1b)

where  $S_N$  is the normalized signal,  $S_F$  and  $S_B$  are the signal contributions from the free (F) and bound (B) populations,  $[P]_T$  and  $[R]_T$  are the total protein (P) and RNA (R) concentration used for the measurement, and  $K_d$  is the equilibrium dissociation constant for the binding reaction.  $K_d$  is related to the Gibbs free energy of binding by the expression  $\Delta G^{\circ}=RT\ln K_D$ , and  $\Delta G^{\circ}$  can be approximated as a linear function of temperature  $\Delta G^{\circ} \approx \delta g_I(T-T_{I/2})$ . The dissociation midpoint temperature  $T_{1/2}$  and  $\delta g_i$  are the fitting parameters. The data analysis was performed in IGOR PRO (fluorometer, WaveMetrics, Lake Oswego, OR) or MATLAB (FReI).

Analysis of Kinetic Data. Relaxation kinetics of binding were collected and plotted as the FRET efficiency vs. time. The resulting transients were fit to the integrated rate law for the bimolecular reaction<sup>22</sup>:

$$\frac{d[PR]}{dt} = -k_{off}[PR] + k_{on}([P]_T - [PR])^2$$
 (2a)

with the solution:

$$t = \frac{2}{\sqrt{k_{off}^2 + 4k_{off}k_{on}[P]_T}} tanh^{-1} \left( \frac{k_{off} + 2k_{on}([P]_T - [PR])}{\sqrt{k_{off}^2 + 4k_{off}k_{on}[P]_T}} \right) \Big|_{[PR]_0}^{[PR]_t} (2b)$$

where  $[P]_T$  is the total protein concentration used for the measurement,  $[PR]_t$  is the complex concentration at time t,  $k_{on}$ is the association rate coefficient, and  $k_{\rm off}$  is the dissociation rate coefficient. The observed signal is proportional to the change in [PR]<sub>t</sub>:

$$A(t) = \sqrt{1 + 4K_d[P]_T} \tag{3a}$$

$$B(t) = tanh\left(\frac{tk_{off}A(t)}{2}\right)$$
 (3b)

$$B(t) = tanh\left(\frac{tk_{off}A(t)}{2}\right)$$

$$C(t) = \frac{1+2K_d([P]_T - [PR]_0)}{A(t)}$$
(3b)

$$S(t) = [P]_T - \frac{1}{2} \left( \left( \frac{B(t) + C(t)}{1 + B(t)C(t)} \right) K_d^{-1} A(t) - K_d^{-1} \right)$$
(3d)

where  $K_d$  is the equilibrium dissociation constant for the binding reaction.  $[PR]_{\theta}$  can be related to Gibbs free energy as described in the Analysis of Thermodynamic Data. Thermodynamic and kinetic FReI data were simultaneously fit to the same  $\delta g_i$  and  $T_{1/2}$  in MATLAB.

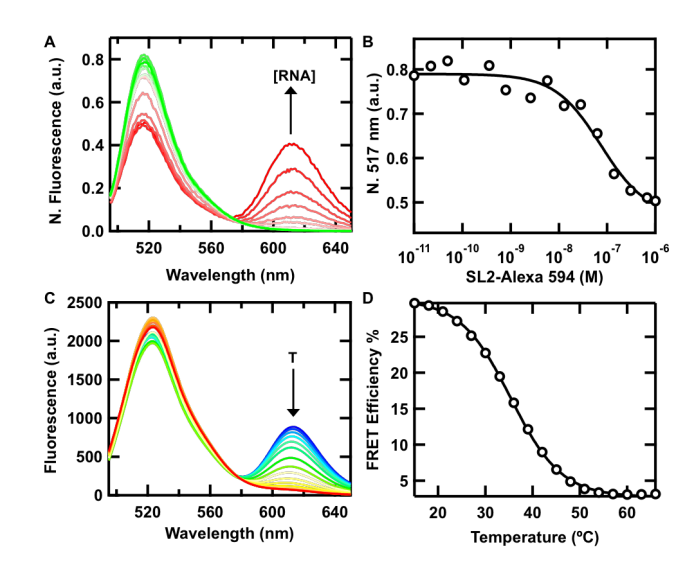
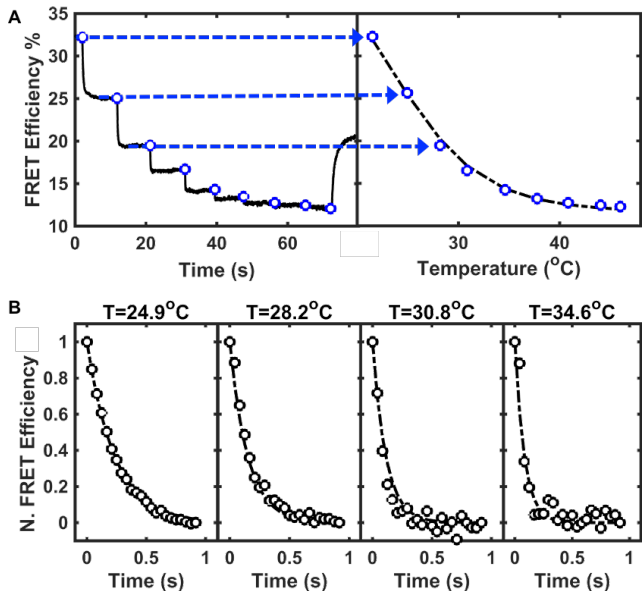


Figure 2. FRET as a probe of U1A-SL2 binding. (A) Fluorescence emission spectra (excitation 488 nm) recorded during the titration of SL2-Alexa 594 into 0.1 µM U1A-Alexa 488 (10 mM potassium phosphate and 200 mM KCl pH 7). SL2-Alexa 594 was added in increments up to 1 µM. The fluorescence emission is normalized to the pre-titration emission of U1A-Alexa 488. (B) N. 517 nm = Normalized change in the fluorescence emission at 517 nm of the FRET binding assay, same arbirary units (a.u.) as in panel (A). A fit to the Hill equation with a Hill coefficient of 1 is overlaid on the data. (C) Temperature induced dissociation of 1 μM U1A-Alexa 488 in complex with 1 μM SL2-Alexa 594 (10 mM potassium phosphate and 200 mM KCl pH 7). Fluorescence emission spectra (excitation 488 nm) collected between 15 and 66 °C in 3 °C intervals. (D) Temperature-dependent FRET efficiency (%) extracted from temperature induced dissociation of U1A-SL2 in (C). The continuous line represents a fit of the data to Equation (1) assuming a 1:1 binding process.

# **RESULTS**

FRET as a Probe of U1A-SL2 Binding. In order to perform binding measurements on U1A-SL2 inside cells, we conjugated Alexa 488 to U1A through a C5-maleimide linkage at 194C and Alexa 594 to the 3' end of SL2 through an NHS ester modification (Figure 1). The in vitro interaction between Alexa labeled U1A-SL2 produces a FRET signal that is sensitive to RNA concentration and temperature (Figure 2). While FRET is sensitive to the distance between the donor and acceptor fluorophores, it does not directly probe binding. To test whether the FRET signal is a direct probe of complex formation, we followed the Alexa labeled U1A-SL2 interaction by tryptophan fluorescence (Figure S1). The ability of U1A F56W fluorescence to report on binding was previously validated by electrophoretic mobility shift assay.<sup>15</sup> The agreement between FRET and tryptophan data (Figure S1) demonstrates that FRET is a probe of the U1A-SL2 binding interaction.



**Figure 3.** Thermodynamics and kinetics extracted from FReI induced dissociation of U1A-SL2. (A) FRET Efficiency of 1 μm U1A-Alexa 488 in complex with 1 μm SL2-Alexa 594 (10 mM potassium phosphate and 200 mM KCl pH 7) during a rapid sequence of temperature jumps. (Left) The FRET efficiency decreases due to dissociation of U1A-SL2. (Right) A temperature titration (o) is extracted from the final 4 seconds of the equilibrium (flat phase) following the jump. Dashed arrows are provided as a guide between equivalent FRET efficiencies during the jump converted to temperature. (B) Relaxation kinetics extracted from the first four temperature jumps. The thermodynamic and kinetic data are globally fit (--) to the temperature-titration (Equation 1) and the integrated rate law (Equation 3), respectively, for the bimolecular reaction.

The binding affinity of Alexa labeled U1A-SL2 was measured in two ways. First, affinity was measured by an equilibrium binding titration; 0.1 µm U1A-Alexa 488 was titrated with SL2-Alexa 594 up to 1 µm (Figure 2A). U1A-Alexa 488 fluorescence decreases 50% over the binding titration (Figure 2B) due to energy transfer to SL2-Alexa 594 upon binding. A fit to the Hill equation determined that U1A-SL2 binds independently with an affinity of  $7.0 \pm 0.2 \times 10^{-8}$  M (error is the standard error of 4 titrations). Second, affinity was measured by an equilibrium temperature titration (Figure 2C). Temperature-dependent measurements of U1A-Alexa 488 alone and SL2-Alexa 594 alone (Figure S2) evaluated the temperature dependence of the labeled constructs. The intensity of U1A-Alexa 488 decreased approximately linearly with increasing temperature, whereas the intensity of SL2-Alexa 594 was temperature independent. Therefore, upon temperatureinduced dissociation of the complex we expect to see a smaller increase in the donor signal than expected from the FRET titration, but a similar change in acceptor intensity. At a constant 1:1 ratio of 1 µm Alexa labeled U1A-S12 complex, dissociation was induced by raising the temperature from 15 to 66 °C. FRET efficiency was reduced by ≈25% upon dissociation. A fit to the fractional saturation for a bimolecular reaction (equation 1) determined that U1A-SL2 binds with an affinity of  $2.3 \pm 0.4 \times 10^{-8}$  M (error is the standard error of 4 measurements), which agrees with the affinity derived from the equilibrium binding titration.

The in vitro binding affinity of the Alexa-labeled system is reduced compared to the wildtype U1A-SL2 system, 8.0 x 10<sup>-1</sup>

 $^{11}$  M, and similar to the reduced  $K_{\rm d}$  of U1A truncated at the I193 position,  $2.0 \times 10^{-8}$  M. $^{10}$  The reduced  $K_{\rm d}$  of truncated U1A is attributed to both loss of stabilizing long-range electrostatic interactions and loss of direct interactions between the RNA and C-terminal tail U1A because the backbone of D92 and I93 can hydrogen bond with C7. $^{10}$  Circular dichroism of U1A-Alexa 488 (Figure S3), labeled at the I94 position, results in a reduced circular dichroism signal at 208 nm, consistent with loss α-helix in the C-terminal tail. $^{23}$  Since the C-terminal tail of U1A-Alexa 488 is unstructured, it is likely more dynamic than wildtype U1A, reducing the number of productive contacts with RNA. The in vitro labeled U1A-SL2 system is our model for in cell comparison.

FReI as a probe of U1A-SL2 binding affinity and kinetics. Two-color FReI imaging of FRET labeled U1A-SL2 allows us to interrogate the binding of the construct. The donor, Alexa 488, is directly excited by blue LED light. The emission from the donor, Alexa 488, and acceptor, Alexa 594, is separated onto a CMOS detector. To perturb the binding equilibrium, a temperature jump is induced by a 2  $\mu$ m infrared laser, which is absorbed by the water and heats the sample.<sup>24</sup> The time evolution of the FRET signal is monitored as the U1A-SL2 complex relaxes to the new free and bound populations at the higher temperature. A computer-controlled infrared laser was programmed to generate 8 successive temperature jumps with an 8 s sample equilibration time between jumps (Figure 3A, left).<sup>25</sup>

FReI measurements were conducted both in vitro and in cells. Three types of analyses were performed on the data: (1) temperature titrations to assess U1A-SL2 binding affinity in analogy to Fig. 2D (Figure 3A, right); (2) temperature jumps to follow binding kinetics (Figure 3B); and (3) spatial segmentation of in-cell data into nucleus and cytoplasm to determine how U1A-SL2 localization in these two compartments, relevant to spliceosomal subunit assembly, <sup>26</sup> impacts binding affinity and kinetics.

U1A-SL2 thermodynamics and kinetics were quantified from the global fits of the temperature titration and binding kinetics data. To build a temperature titration from the temperature jump data, the FRET efficiency was averaged over the equilibrated final 4 seconds following the jump (Figure 3A). This data is equivalent to temperature titrations collected on a fluorometer (Figure 2D). Relaxation kinetics were extracted from the first second of the

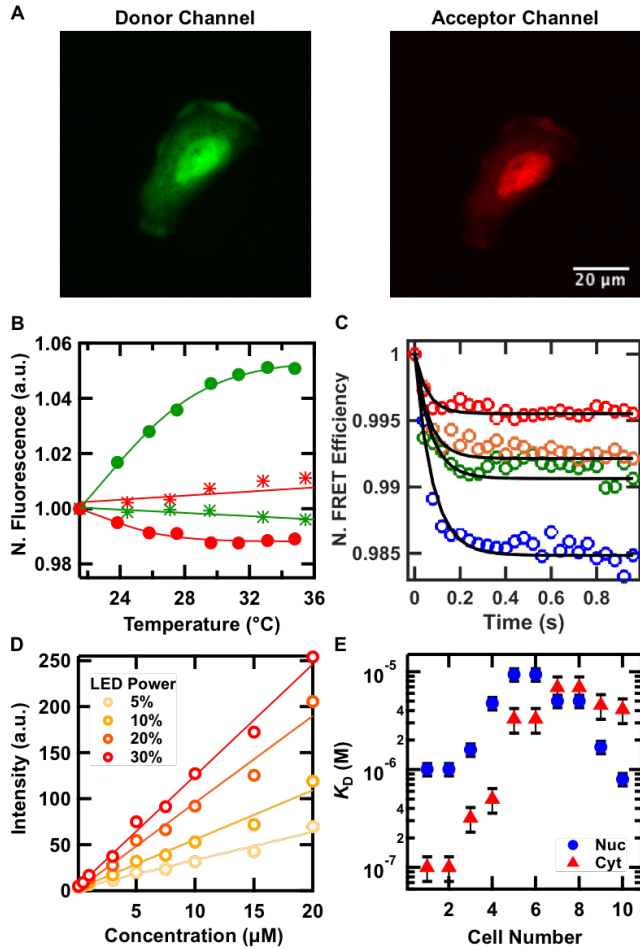


Figure 4. Binding affinity and rate coefficients measured in living cells. (A) Donor and acceptor channels shown after microinjection of 1:1 ratio of U1A-Alexa 488 and SL2-Alexa 594 into a U-2 OS cell. Scale bar is 20 µm. (B) Temperature dependence of free U1A-Alexa 488 (green asterisks), free SL2-Alexa 594 (red asterisks), and pre-complexed U1A-Alexa 488 and SL2-Alexa 594 (red and green circles) microinjected into a U-2 OS cell. Data is extracted from the final 4 seconds of equilibration (flat phase) following the T-jump. A linear (free) and sigmoid (complex) fit are overlaid on the data to highlight differences in the temperature dependence. (C) Relaxation kinetics extracted from the first four T-jumps (blue 23.8 °C, green 25.8 °C, orange 29.6 °C, and red 31.3 °C). A global fit to Equation 3 is overlaid on the data. (D) Concentration calibration curves of SL2-Alexa 594 (10 mM potassium phosphate and 200 mM KCl pH 7) using a 10 µm spacer to mimic the pathlength of the cell. All in-cell measurements were carried out at LED intensities between 5 and 30% power. (E) Equilibrium dissociation constant  $(K_d)$  measured in the nucleus and cytoplasm of the same cell. To determine  $K_d$  and rate coefficient for the bimolecular reaction, the thermodynamics and kinetics are extracted from the nucleus or cytoplasm of each individual cell and globally fit to the temperature-titration (Equation 1) and the integrated rate law (Equation 3), respectively.

first four temperature jumps (Figure 3B). Each jump is of  $\approx$ 3 °C and has a time resolution of  $\approx$ 100 ms. The thermodynamic and kinetic data are globally fit to the temperature titration (Equation 1) and integrated rate law (Equation 3), respectively, for the bimolecular U1A-SL2 reaction. FReI determined that U1A-SL2 binds *in vitro* with an affinity of  $7.0 \pm 0.5 \times 10^{-8}$  M,  $k_{\rm on}$ =  $1.13 \pm 0.01 \times 10^{7}$  M<sup>-1</sup>s<sup>-1</sup>, and  $k_{\rm off}$ =  $8.3 \pm 0.5 \times 10^{-1}$  s<sup>-1</sup> (error is the standard error of 4 measurements). This agrees

with the fluorometer assessed affinities, validating the T-jump approach to quantify binding affinity and kinetics.

Binding measurements in living cells. U1A-Alexa 488, SL2-Alexa 594, or a 1:1 mixture of pre-complexed labeled U1A-SL2 (Figure 4A) was microinjected into U-2 OS cells and allowed to equilibrate. The temperature dependences of U1A-Alexa 488 fluorescence intensity alone (excitation 450-490 nm) and SL2-Alexa 594 alone (excitation 565-598 nm) were decreasing and increasing, respectively. Over the temperature range of our FReI studies the intensities are approximately linear with a <1% change in intensity (Figure 4B). By contrast, the temperature dependence of the dyes on the U1A-SL2 complex follow the

opposite trend, the change in intensities are sigmoidal and significantly larger. This indicates that the change in FRET signal is specific for U1A-SL2 binding.

Determination of U1A-SL2 Concentration in Cells. The observed temperature-jump kinetics of bimolecular processes are dependent on the association rate coefficient, dissociation rate coefficient, and the protein concentration. Therefore, to properly fit the data, it is necessary to quantify the intracellular protein concentrations. Each cell was segmented into the nucleus and cytoplasm (see Methods) and a calibration curve was used to determine the sub-cellular concentrations.

Calibration curves of in vitro SL2-Alexa 594 (Figure 4D) were generated using amber excitation (565-598 nm) and the acceptor channel of the FReI microscope. To match the pathlength (height) of U-2 OS cells, the concentration dependent SL2-Alexa 594 intensity was monitored in an imaging chamber with a 10  $\mu m$  spacer. The height of U-2 OS cells under our measurement conditions,  $10 \pm 2~\mu m$ , was determined using a confocal microscope. Since the LED power is adjusted to maximize the signal of each in-cell measurement, calibration curves were generated for LED settings between 5 and 30% power.

The same calibration curve was used to calculate the concentration of U1A-Alexa 488 and SL2-Alexa 594 complexed inside cells. The concentration of SL2-Alexa 594 alone or in complex can be directly determined from the calibration curve. To correct for the cellular background, the average background intensity was subtracted from the average nucleus and average cytoplasmic intensity. In general, this correction was ≈0.6 µM per cell and at least an order of magnitude smaller than the uncorrected concentration. U1A-Alexa 488 was not used to calculate concentrations, because when complexed its intensity is altered by FRET. Instead, the protein and RNA were microinjected at a 1:1 ratio, ensuring that the U1A-Alexa 488 and SL2-Alexa 594 concentrations are the same. In principle, a systematic under-estimation of the cellular concentration of U1A and SL2 in cells could reproduce the discrepancy between in cell and in vitro measurements presented here. However, this would require a two order of magnitude decrease in the concentrations, which is far below the detection limit of our microscope. Measured concentrations were in a range of 5-35  $\mu$ M in the nucleus and 5-15  $\mu$ M in the cytoplasm (Table S1).

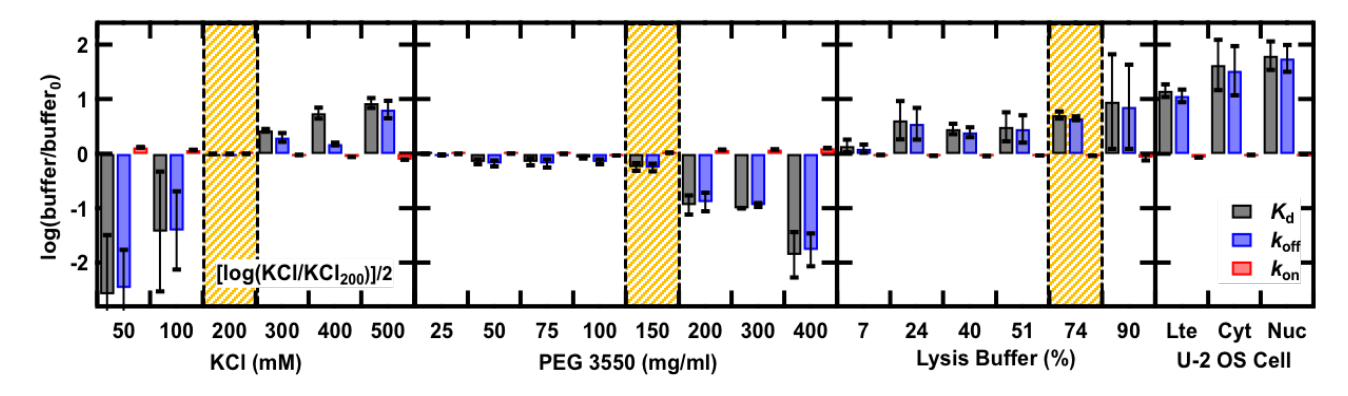


Figure 5. Effect of electrostatic, crowding, and chemical interactions on  $K_d$ ,  $k_{off}$ , and  $k_{on}$ . To visualize differences between electrostatic screening (KCl), crowding (PEG 3550), and cell-mimic chemical interactions (Pierce IP lysis buffer) conditions and our standard buffer (200 mM KCl: 10 mM potassium phosphate and 200 mM KCl pH 7), we plotted the logarithm of the buffer/standard buffer  $K_d$  (black),  $k_{off}$  (blue), and  $k_{on}$  (red) values. Also presented are measurements collected in U-2 OS cell lysate (Lte) and measurements averaged over the cytoplasm (Cyt) and nucleus (Nuc) of a living U-2 OS cell. Buffer conditions that best replicate the cellular environment (200 mM KCl, 150 mg/ml PEG 3550, and 74% lysis buffer) are shaded tan. So that all data can be visualized on the same y-axis, KCl data are scaled by ×0.5. Error bars indicate the standard deviation of three experiments in vitro, ≈30 measurements in the nucleus, and ≈10 measurements in the cytoplasm.

Binding affinities, association and dissociation rate coefficients of U1A-SL2 in living cells. Each cell contains an equal concentration of U1A-Alexa 488 and SL2-Alexa 594. Therefore, the integrated rate law for the bimolecular reaction can be simplified to the model for a dimerization reaction (see Methods). The observed thermodynamics and kinetics were globally fit to the temperature titration (Equation 1) and integrated rate law (Equation 3) at the measured U1A and SL2 concentration.

The binding affinities measured in the nucleus and cytoplasm were similar:  $4.4 \pm 0.6 \times 10^{-6} \, \text{M}$  and  $3.0 \pm 0.8 \times 10^{-6} \, \text{M}$ , respectively (Table S1). In 80% of cells tested, the apparent binding affinity measured in the nucleus was equal to or weaker than that measured in the cytoplasm (Figure 4E). U1A-SL2 dissociated slightly faster in the nucleus and there was no significant difference in the association rate coefficient (Table S1).

Binding affinities and rate coefficients are intrinsic properties of the complex, therefore differences must be due to local environmental differences (e.g. salt, pH, crowding) and not concentration dependent. Indeed, as anticipated no correlation was found between the complex concentration and the apparent binding affinity (Figure S4).

Environmental differences between the nucleus and cytoplasm (and in vitro) can be attributed to differences in steric crowding and non-steric electrostatic and sticking effects. The cytoplasm of eukaryotic cells is slightly more crowded than the nucleus.<sup>27–29</sup> Macromolecular composition varies by compartment; deep UV-microscopy revealed nucleic acids, ≈ 35 mg/ml, are heavily concentrated in the nucleus, whereas protein concentration is high throughout the cell,  $\approx 150$ mg/ml.<sup>30,31</sup> Small molecules and ions are able to pass freely through the nuclear envelope; neither an electrochemical potential nor osmotic gradient is established between the nucleus and cytoplasm.<sup>32</sup> However, there is a pH gradient with a slightly higher pH found in the nucleus. 33,34 To disentangle somewhat the contributions of crowding, electrostatics, and sticking to U1A-SL2 binding affinity and rate coefficients measured inside cells we mimicked steric and non-steric effects in vitro.

Mimicking the in-cell environment in vitro. The initial buffer condition for in vitro measurements, 10 mM potassium phosphate and 200 mM potassium chloride pH 7, was selected to replicate the ionic strength of the cell.<sup>35</sup> Compared to in vitro measurements in 200 mM KCl, U1A-SL2 had a binding affinity up to two orders of magnitude weaker inside cells (Table S1). There is little difference in the observed association rate coefficient, instead the difference in binding affinity arises from up to a two order of magnitude increase in the dissociation rate coefficient.

We considered three conditions that may contribute to binding differences inside cells, each with a different balance of steric and non-steric effects: (1) Electrostatic screening by cellular electrolytes can perturb the binding interaction between the highly charged protein and RNA through ionspecific binding or non-specific ionic screening. (2) Steric interactions are mimicked in vitro by the crowding agent polyethylene glycol, PEG 3550. PEG is commonly used to mimic cellular crowding.<sup>36</sup> (3) Lysis buffer or dilute cell lysate mimic the non-steric sticking interactions with small organics molecules. osmolytes. and macromolecular cellular components.<sup>37,38</sup> A complete table of in vitro and in-cell measurements can be found in Table S2 and Table S1, respectively.

Perturbations to the ionic strength had the largest effect on in vitro binding affinity and rate coefficients (Figure 5). The net concentration of ions in the cell is  $\approx 200$  mM and K<sup>+</sup> is the most common ion in the intracellular fluid, <sup>35</sup> therefore the ionic composition is mimicked in vitro by KCl. The effect of KCl on binding was tested between 50 and 500 mM. As anticipated, increasing the salt concentration decreases the affinity of U1A-SL2. Salt also increased the dissociation rate coefficient. However, the KCl concentration necessary to yield a cell-like result,  $\geq 500$  mM, does not fall near physiological salt concentrations (shaded tan, Figure 5).

Differences between in vitro and in cell U1A-SL2 affinity also cannot be explained by steric crowding. Excluded-volume theory predicts that steric crowding stabilizes complexes.<sup>39</sup> Therefore, we anticipate that macromolecular crowding cannot

explain the reduced binding affinity observed inside cells. Since physiological concentrations of macromolecules can be as high as 300-400 mg/ml, <sup>40</sup> crowding was tested to a maximum of 400 mg/ml. Indeed, increased crowding produced the opposite trend from what we observe inside cells (Figure 5). At crowding conditions that approximately match physiological conditions, 150 mg/ml (shaded tan, Figure 5), binding affinity and dissociation rate coefficients are reduced compared to in vitro and in cells.

Finally we compared the binding affinity and rate coefficients in lysis buffer and cell lysates, which mimic non-steric sticking effects. Pierce IP lysis buffer contains ions (150 mM NaCl), small organics (25 mM tris, 5% glycerol, 1 mM EDTA) and short-chain fatty acid mimics (1% NP-40). Lysis buffer was established in the past as a good mimic for in-cell effects on protein folding.<sup>37,38</sup> Likewise, measurements in lysis buffer produce the correct stability and kinetic trends (Figure 5). However, quantitative agreement is not achieved in 74% lysis buffer (shaded tan, Figure 5), the condition previously found to best reproduce in-cell protein stability trends.<sup>37,38</sup> Even at the highest lysis buffer concentration we tested the incell affinity and rates are not yet reached.

Non-specific sticking of macromolecules may also contribute to the observed binding affinity and kinetics.<sup>41</sup> To test whether non-specific interactions with macromolecules contribute to the observed in-cell binding affinity and rate coefficients, cell lysate was prepared from U-2 OS cells. Measurements in dilute cell lysate (Figure 5) extended the trend observed in lysis buffer and most closely reproduced the in-cell observations. This suggests that non-specific sticking interactions between the cellular matrix and the complex and/or individual binding partners are responsible for the reduced affinity and dissociation rate coefficient observed inside cells.

#### DISCUSSION

Nonspecific sticking of the complex reduces binding inside cells. It is not simply affinity, but specificity that is critical to maintaining cellular function. It is relatively easy to produce a strong interaction between N-2 binding partners, but much harder to simultaneously avoid the collective effect of many weak interactions in a cell filled with M>>2 potential binding partners. Each one of the M>>N undesirable interactions may have a very small  $\Delta G$  compared to the few desired interactions, but the sheer number of undesirable interactions will interfere with the desirable interaction and shift the apparent binding constant.

Indeed, our measured binding affinity and rates for U1A-SL2 in vitro agree well with literature data from other solution measurements,  $^{10,42,43}$  but binding is significantly weakened inside cells. Surprisingly, despite up to a two order of magnitude decrease in affinity in cells, the association rate coefficient  $k_{on}$  was essentially unperturbed inside cells. This parallels previous measures of association rate coefficients inside cells, where variations occurred within a small window around the in vitro measurements.  $^{3,44-46}$  Finally, we observe that the increase of  $K_d$  is similar in the nucleus and cytoplasm, so a fairly generic effect seems to be at play, not a nucleus- or cytoplasm-specific interaction. To understand our observations, we consider three general factors that modulate binding affinity and rates inside cells: electrostatic screening, crowding, and non-specific interactions.

Electrostatic interactions differently affect the stability of the reactants, complex, and intermediate structures.<sup>47</sup> Therefore, although repulsive electrostatic interactions are destabilizing, the overall effect depends on the relative free energies of the different states. For example, ionic shielding enhances binding and association rates in DNA hybridization<sup>46</sup> and ionic screening destabilizes U1A-SL2 binding and association rates.<sup>42,48</sup> Although ionic screening of U1-SL2 produces the correct affinity and rate trends (Figure 5), non-physiological conditions are necessary to reproduce the observed in-cell binding effects. Thus screening alone cannot be the whole story.

Macromolecular crowding can also produce competing effects on the complex: (1) excluded volume predicts that complexes are stabilized and association rates accelerated due to the enhanced effective concentration.<sup>47</sup> (2) however, macromolecular crowding hinders diffusion, potentially slowing association rates. Our study is consistent with recent work shows that macromolecular crowding has little effect on the association rate.<sup>3,49</sup> Therefore, macromolecular crowding cannot explain the decreased U1A-SL2 affinity observed inside cells.

The closest approximation of in-cell U1A-SL2 binding and kinetics is observed in the mimics of non-specific interactions, lysis buffer and cell lysate (Figure 5). Weak non-specific chemical interactions between molecules are pervasive in the cell.<sup>50</sup> These interactions can suppress or activate binding.<sup>51</sup> We and others<sup>3</sup> find that cell lysates best parallel in-cell measurements. Nonspecific interactions can reduce association rates by occupying binding sites and hence reducing the available concentration of binding sites<sup>46,52</sup> or by regulating diffusion rates<sup>53</sup>. Both of these effects would decrease  $k_{on}$ . Yet, the nearly two order of magnitude decrease in U1A-SL2 binding is due to an increase in the dissociation rate coefficient.

To reconcile differences between the expected and observed rate coefficients we built a minimal reaction model that reproduces all our in vitro and in-cell data by incorporating nonspecific binding (Scheme 1). The minimal model capable of reproducing the observed in-cell affinity includes five reversible reactions: The first reaction ( $k_{on}$  and  $k_{off}$ ) is equivalent to the in vitro reaction of free U1A and RNA to form the bound complex. These rate coefficients were fixed to the values measured in vitro. The second reaction (k'on and k'off) accounts for complex formation from partners that are transiently sticking to the intracellular matrix by non-specific interactions. The remaining three reactions (k) allow the free and transiently sticking species to interconvert, reducing the concentration of free monomer and complex in the cell. For simplicity we fixed the forward and reverse sticking reactions at the same value of k, enforcing an even equilibrium between free and matrix-bound species. Also for simplicity, we treat both A and B species in the parallel reaction at the bottom as sticking, although a similar fit can be obtained even if only one of them sticks and the other remains free. There are now two ways that  $K_d$  can be reduced: if  $k'_{on} < k_{on}$ , binding is reduced in the cell because the reactants are not binding as quickly; if  $k'_{\text{off}} > k_{\text{off}}$ , binding is reduced in the cell because the complex AB itself is weakened by sticking interactions forming AB<sub>sticks</sub>. Although we cannot uniquely define k, a k of 1000 s<sup>-1</sup> and  $k'_{on}=k_{on}$  and  $k'_{off}=5$   $k'_{off}$ accounts for the observed scenario of a 100-fold larger  $K_d$  and apparent dissociation rate coefficient, but scenarios with  $k'_{on}$  $< k_{\rm on}$  do not.

#### Scheme 1. In-cell U1A-SL2 binding model

Thus two effects are responsible for the apparent weakening of the U1A-SL2 complex: (1) non-specific interactions reduce the concentration of free U1A and SL2 that would form a strongly bound free complex. (2) Still productive, but weaker interactions between U1A and SL2 non-specifically bound to the cellular environment form a complex just as easily as before (same  $k_{on}$ ), but the complex is less stable (greater  $k_{off}$ ). The underlying cause is likely that charged small solute and macromolecular non-specific binders of U1A and SL2, both highly charged molecules, screen some of the electrostatic interactions between the protein and RNA, and while not interfering with the specificity of the complex, reduce its stability. This is strongly supported by in vitro mutation experiments that have shown how the U1A-SL2 interaction is weakened by charge-reducing interactions on the U1A protein, 48,54 while maintaining a similar bound complex structure in molecular dynamics simulations.

This interpretation would predict that species without strong surface interactions (low charge, no large hydrophobic patches) will suffer less interference from the cellular matrix than species with strong surface interactions. This could be one reason why disorder of unbound intrinsically disordered proteins (IDPs) that 'bind and fold' can be advantageous: the larger unbound state disperses the sticking interaction of a highly localized large charge.

For the same reasons, we expect that the in-cell sticking to complexes assembled from highly charged components will also strongly modulate their ability to segregate into liquidliquid phase separated regions (LLPSRs). Indeed, at concentrations higher than the present study, we observe (Figure 6) that U1A protein and SL2 RNA do form phase-separated regions reversibly and exclusively in the nucleus of U-2 OS cells. These LLPSRs are highly temperature sensitive with a transition not far from body temperature. The nuclear concentration of U1 complexes is tightly regulated; upon dissolution of LLPSRs the nuclear concentration of U1A is constant, and excess "dissolved" protein is exported to the cytoplasm. This may be important both to ensure that should U1A dissociate from the U1 snRNP it can reform the complex, and to prevent interactions between U1A and the many other RNAs in the nucleus. Thus U1A and SL2 are poised to form macroscopic associations not far from physiological conditions inside the cell, and small differences in the local interactions control whether LLPSRs form or not.

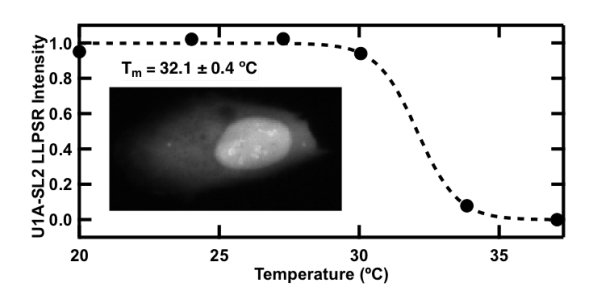


**Figure 6.** Effect of temperature on stability of U1A-SL2 liquid-liquid phase separated regions in a U-2 OS nucleus. There is a sharp phase transition at 32 °C, above which the Cajal-body-like LLPSRs in the nucleus dissolve. The dissolution is reversible when the temperature is lowered again.

# CONCLUSION AND OUTLOOK

The affinity and rate coefficients for many cellular interactions are determined in dilute aqueous conditions in a test tube and the accuracy of the measurements in the cellular environment is never tested. Similarly, drug interactions are optimized to high affinity, but may be much lower in the cell environment. Although we study a specific system here, this approach can be applied broadly to any bimolecular interaction with relaxation time >100 ms in adhered cells. Our results highlight the importance of studying bimolecular processes in their native cellular environment; we observe up to two orders of magnitude differences in the apparent affinity and complex dissociation rate coefficient inside cells. Tight binding affinities observed or designed in vitro may be necessary to compete with non-specific interactions in the cellular environment, in particular when strongly interacting species are involved, such as nucleic acids or highly charged globular or disordered proteins.

# ASSOCIATED CONTENT

# **Supporting Information**

The Supporting Information is available free of charge on the ACS Publications website.

Plots of representative temperature induced dissociation monitored by tryptophan fluorescence and FRET, circular dichroism of labeled and unlabeled U1A,  $K_d$  measured in the nucleus and cytoplasm of U-2 OS cells, and complete tables of thermodynamic and kinetic parameters obtained in vitro and in living U-2 OS cells. (PDF)

#### **AUTHOR INFORMATION**

#### **Corresponding Authors**

\* c.davis@yale.edu, mgruebel@illinois.edu

# **Present Addresses**

† Department of Chemistry, Yale University, 225 Prospect St., New Haven, CT, 06520 USA

# **Author Contributions**

The manuscript was written through contributions of all authors. All authors have given approval to the final version of the manuscript.

#### **Funding Sources**

This work was supported by the National Institutes of Health grant R01GM093318 (in vitro work) and National Science Foundation (NSF) grant NSF MCB 1803786 (in-cell work) to M.G. C.M.D. was supported in part by a postdoctoral fellowship provided by the PFC: Center for the Physics of Living Cells funded by NSF PHY 1430124.

#### Notes

The authors declare no competing financial interest.

# **ACKNOWLEDGMENT**

The authors thank Irisbel Guzman Sanchez and David Gnutt for helpful discussion and initiating the project.

# REFERENCES

- Sukenik, S.; Ren, P.; Gruebele, M. Weak Protein–Protein Interactions in Live Cells Are Quantified by Cell-Volume Modulation. *Proc. Natl. Acad. Sci. U. S. A.* 2017, 114, 6776– 6781.
- (2) König, I.; Zarrine-Afsar, A.; Aznauryan, M.; Soranno, A.; Wunderlich, B.; Dingfelder, F.; Stüber, J. C.; Plückthun, A.; Nettels, D.; Schuler, B. Single-Molecule Spectroscopy of Protein Conformational Dynamics in Live Eukaryotic Cells. Nat. Methods 2015, 12, 773–779.
- (3) Phillip, Y.; Kiss, V.; Schreiber, G. Protein-Binding Dynamics Imaged in a Living Cell. Proc. Natl. Acad. Sci. U. S. A. 2012, 109, 1461–1466.
- (4) Kwapiszewska, K.; Kalwarczyk, T.; Michalska, B.; Szczepański, K.; Szymański, J.; Patalas-Krawczyk, P.; Andryszewski, T.; Iwan, M.; Duszyński, J.; Hołyst, R. Determination of Oligomerization State of Drpl Protein in Living Cells at Nanomolar Concentrations. Sci. Rep. 2019, 9, 5006
- (5) Schreiber, G.; Haran, G.; Zhou, H.-X. Fundamental Aspects of Protein-Protein Association Kinetics. Chem. Rev. 2009, 109, 839–860
- (6) Carroll, M. J.; Mauldin, R. V.; Gromova, A. V.; Singleton, S. F.; Collins, E. J.; Lee, A. L. Evidence for Dynamics in Proteins as a Mechanism for Ligand Dissociation. *Nat. Chem. Biol.* 2012, 8, 246–252.
- (7) Lu, H.; Tonge, P. J. Drug–Target Residence Time: Critical Information for Lead Optimization. Curr. Opin. Chem. Biol. 2010, 14, 467–474.
- (8) Campbell, C. S.; Mullins, R. D. In Vivo Visualization of Type II Plasmid Segregation: Bacterial Actin Filaments Pushing Plasmids. J. Cell Biol. 2007, 179, 1059–1066.
- (9) Bouzo-Lorenzo, M.; Stoddart, L. A.; Xia, L.; IJzerman, A. P.; Heitman, L. H.; Briddon, S. J.; Hill, S. J. A Live Cell NanoBRET Binding Assay Allows the Study of Ligand-Binding Kinetics to the Adenosine A3 Receptor. *Purinergic Signal*. 2019, 15, 139–153.
- (10) Zeng, Q.; Hall, K. B. Contribution of the C-Terminal Tail of U1A RBD1 to RNA Recognition and Protein Stability. RNA 1997, 3, 303–314.
- (11) Hall, K. B.; Stump, W. T. Interaction of N-Terminal Domain of U1a Protein with an Rna Stem Loop. *Nucleic Acids Res.* 1992, 20, 4283–4290.
- (12) Showalter, S. A.; Hall, K. B. Correlated Motions in the U1 SnRNA Stem/Loop 2:U1A RBD1 Complex. *Biophys. J.* 2005, 89, 2046–2058.
- (13) Humphrey, W.; Dalke, A.; Schulten, K. VMD: Visual Molecular Dynamics. J. Mol. Graph. 1996, 14, 33–38.
- (14) Nagai, K.; Oubridge, C.; Jessen, T. H.; Li, J.; Evans, P. R. Crystal Structure of the RNA-Binding Domain of the U1 Small Nuclear Ribonucleoprotein A. *Nature* 1990, 348, 515–520.
- (15) Anunciado, D.; Dhar, A.; Gruebele, M.; Baranger, A. M. Multistep Kinetics of the U1A-SL2 RNA Complex Dissociation. J. Mol. Biol. 2011, 408, 896–908.
- (16) Ghaemi, Z.; Guzman, I.; Gruebele, M.; Luthey-Schulten, Z. Electrostatic Interaction Effects on the Binding of Spliceosomal U1A Protein-SL2 RNA Hairpin. *Biophys. J.* 2015, 108, 15a-15a.
- (17) Guzman, I.; Ghaemi, Z.; Baranger, A.; Luthey-Schulten, Z.;

- Gruebele, M. Native Conformational Dynamics of the Spliceosomal U1A Protein. J. Phys. Chem. B 2015, 119, 3651–3661
- (18) Kisley, L.; Serrano, K. A.; Guin, D.; Kong, X.; Gruebele, M.; Leckband, D. E. Direct Imaging of Protein Stability and Folding Kinetics in Hydrogels. ACS Appl. Mater. Interfaces 2017, 9, 21606–21617.
- (19) Dhar, A.; Girdhar, K.; Singh, D.; Gelman, H.; Ebbinghaus, S.; Gruebele, M. Protein Stability and Folding Kinetics in the Nucleus and Endoplasmic Reticulum of Eucaryotic Cells. *Biophys. J.* 2011, 101, 421–430.
- (20) Otsu, N. A Threshold Selection Method from Gray-Level Histograms. *IEEE Trans. Syst. Man. Cybern.* **1979**, *9*, 62–66.
- (21) Pollard, T. D. A Guide to Simple and Informative Binding Assays. Mol. Biol. Cell 2010, 21, 4061–4067.
- (22) Korobov, V. I.; Ochkov, V. F. Multi-Step Reactions: The Methods for Analytical Solving the Direct Problem. In *Chemical Kinetics with Mathcad and Maple*; Springer Vienna: Vienna, 2011; pp 35–72.
- (23) Jean, J. M.; Clerte, C.; Hall, K. B. Global and Local Dynamics of the Human U1A Protein Determined by Tryptophan Fluorescence. *Protein Sci.* 1999, 8, 2110–2120.
- (24) Kubelka, J. Time-Resolved Methods in Biophysics. 9. Laser Temperature-Jump Methods for Investigating Biomolecular Dynamics. *Photochem. Photobiol. Sci.* 2009, 8, 499–512.
- (25) Guo, M.; Xu, Y.; Gruebele, M. Temperature Dependence of Protein Folding Kinetics in Living Cells. *Proc. Natl. Acad. Sci.* U. S. A. 2012, 109, 17863–17867.
- (26) Matera, A. G.; Wang, Z. A Day in the Life of the Spliceosome. Nat. Rev. Mol. Cell Biol. 2014, 15, 108–121.
- (27) Guigas, G.; Kalla, C.; Weiss, M. The Degree of Macromolecular Crowding in the Cytoplasm and Nucleoplasm of Mammalian Cells Is Conserved. FEBS Lett. 2007, 581, 5094–5098.
- (28) Schürmann, M.; Scholze, J.; Müller, P.; Guck, J.; Chan, C. J. Cell Nuclei Have Lower Refractive Index and Mass Density than Cytoplasm. J. Biophotonics 2016, 9, 1068–1076.
- (29) Guigas, G.; Kalla, C.; Weiss, M. Probing the Nanoscale Viscoelasticity of Intracellular Fluids in Living Cells. *Biophys.* J. 2007, 93, 316–323.
- (30) Zeskind, B. J.; Jordan, C. D.; Timp, W.; Trapani, L.; Waller, G.; Horodincu, V.; Ehrlich, D. J.; Matsudaira, P. Nucleic Acid and Protein Mass Mapping by Live-Cell Deep-Ultraviolet Microscopy. Nat. Methods 2007, 4, 567–569.
- (31) Cheung, M. C.; LaCroix, R.; McKenna, B. K.; Liu, L.; Winkelman, J.; Ehrlich, D. J. Intracellular Protein and Nucleic Acid Measured in Eight Cell Types Using Deep-Ultraviolet Mass Mapping. Cytom. Part A 2013, 83A, 540–551.
- (32) Richter, K.; Nessling, M.; Lichter, P. Macromolecular Crowding and Its Potential Impact on Nuclear Function. *Biochim. Biophys.* Acta - Mol. Cell Res. 2008, 1783, 2100–2107.
- (33) Seksek, O.; Bolard, J. Nuclear PH Gradient in Mammalian Cells Revealed by Laser Microspectrofluorimetry. J. Cell Sci. 1996.
- (34) Masuda, A.; Oyamada, M.; Nagaoka, T.; Tateishi, N.; Takamatsu, T. Regulation of Cytosol–Nucleus PH Gradients by K+/H+ Exchange Mechanism in the Nuclear Envelope of Neonatal Rat Astrocytes. *Brain Res.* 1998, 807, 70–77.
- (35) Ames, A.; Nesbett, F. B.; Nesbett, F. B. Intracellular and Extracellular Compartments of Mammalian Central Nervous Tissue. J. Physiol. 1966, 184, 215–238.
- (36) Phillip, Y.; Sherman, E.; Haran, G.; Schreiber, G. Common Crowding Agents Have Only a Small Effect on Protein-Protein Interactions. *Biophys. J.* **2009**, *97*, 875–885.
- (37) Davis, C. M.; Gruebele, M. Non-steric Interactions Predict the Trend and Steric Interactions the Offset of Protein Stability in Cells. ChemPhysChem 2018, 19, 2290–2294.
- (38) Davis, C. M.; Deutsch, J.; Gruebele, M. An in Vitro Mimic of In-cell Solvation for Protein Folding Studies. *Protein Sci.* 2020, 29, 1046–1054.
- (39) Minton, A. P. Excluded Volume as a Determinant of Protein Structure and Stability. *Biophys. J.* **1980**, *32*, 77–79.
- (40) Zimmerman, S. B.; Trach, S. O. Estimation of Macromolecule Concentrations and Excluded Volume Effects for the Cytoplasm of Escherichia Coli. *J. Mol. Biol.* 1991, 222, 599–620.
- (41) Cohen, R. D.; Pielak, G. J. Electrostatic Contributions to Protein Quinary Structure. J. Am. Chem. Soc. 2016, 138, 13139–13142.

- (42) Qin, S.; Zhou, H.-X. Prediction of Salt and Mutational Effects on the Association Rate of U1A Protein and U1 Small Nuclear RNA Stem/Loop II †. J. Phys. Chem. B 2008, 112, 5955–5960.
- (43) Law, M. J. The Role of RNA Structure in the Interaction of U1A Protein with U1 Hairpin II RNA. RNA 2006, 12, 1168–1178.
- (44) Kozer, N.; Schreiber, G. Effect of Crowding on Protein–Protein Association Rates: Fundamental Differences between Low and High Mass Crowding Agents. J. Mol. Biol. 2004, 336, 763–774.
- (45) Kozer, N.; Kuttner, Y. Y.; Haran, G.; Schreiber, G. Protein-Protein Association in Polymer Solutions: From Dilute to Semidilute to Concentrated. *Biophys. J.* 2007, 92, 2139–2149.
- (46) Schoen, I.; Krammer, H.; Braun, D. Hybridization Kinetics Is Different inside Cells. Proc. Natl. Acad. Sci. 2009, 106, 21649– 21654
- (47) Minton, A. P. How Can Biochemical Reactions within Cells Differ from Those in Test Tubes? J. Cell Sci. 2006, 119, 2863– 2869.
- (48) Law, M. J. The Role of Positively Charged Amino Acids and Electrostatic Interactions in the Complex of U1A Protein and U1 Hairpin II RNA. Nucleic Acids Res. 2006, 34, 275–285.
- (49) Wieczorek, G.; Zielenkiewicz, P. Influence of Macromolecular Crowding on Protein-Protein Association Rates—a Brownian

- Dynamics Study. Biophys. J. 2008, 95, 5030-5036.
- (50) Deeds, E. J.; Ashenberg, O.; Gerardin, J.; Shakhnovich, E. I. Robust Protein Protein Interactions in Crowded Cellular Environments. Proc. Natl. Acad. Sci. 2007, 104, 14952–14957.
- (51) Demott, C. M.; Majumder, S.; Burz, D. S.; Reverdatto, S.; Shekhtman, A. Ribosome Mediated Quinary Interactions Modulate In-Cell Protein Activities. *Biochemistry* 2017, 56, 4117–4126.
- (52) Jiao, M.; Li, H.-T.; Chen, J.; Minton, A. P.; Liang, Y. Attractive Protein-Polymer Interactions Markedly Alter the Effect of Macromolecular Crowding on Protein Association Equilibria. *Biophys. J.* 2010, 99, 914–923.
- (53) Wang, Y.; Li, C.; Pielak, G. J. Effects of Proteins on Protein Diffusion. J. Am. Chem. Soc. 2010, 132, 9392–9397.
- (54) Ghaemi, Z.; Guzman, I.; Baek, J. J.; Gruebele, M.; Luthey-Schulten, Z. Estimation of Relative Protein–RNA Binding Strengths from Fluctuations in the Bound State. J. Chem. Theory Comput. 2016, 12, 4593–4599.

Authors are required to submit a graphic entry for the Table of Contents (TOC) that, in conjunction with the manuscript title, should give the reader a representative idea of one of the following: A key structure, reaction, equation, concept, or theorem, etc., that is discussed in the manuscript. Consult the journal's Instructions for Authors for TOC graphic specifications.

# Insert Table of Contents artwork here

